

PROBING FREQUENCY-DEPENDENT HALF-WAVE PLATE SYSTEMATICS FOR CMB EXPERIMENTS WITH FULL-SKY BEAM CONVOLUTION SIMULATIONS

Presented by: Matteo Billi

In collaboration with A. Duivenvoorden, A. Adler,
N. Dachlythra and Jón E. Guðmundsson.

CMB-CAL 2024 @Bicocca

November 7, 2024



Università
di Catania



INAF
ISTITUTO NAZIONALE
DI ASTROFISICA

HALF-WAVE PLATE

In CMB polarisation observations residuals of instrumental systematics have to be carefully measured:
spurious signals caused by lack of suitable astrophysical calibration sources
in the microwave frequency band



HALF-WAVE PLATE: POLARISATION MODULATOR

Optical element, composed by birefringent material (sapphire plates), that produces a half-wave phase delay of the incoming radiation

- **IDEAL HWP**: ONLY MODULATES POLARISED SKY SIGNAL
- **REAL HWP**: CAUSE SPURIOUS POLARISED SIGNAL

CURRENT MISSIONS:

MAXIPOL, POLARBEAR, ABS,
SPIDER, EBEX, SO (SAT)

FUTURE MISSIONS:

LiteBIRD

HWP SYSTEMATICS WITH *beamconv*

beamconv (2018)

Duivenvoorden et al., MNRAS (2019)

¹<https://github.com/AdriJD/beamconv>



- Open-source spherical harmonic beam convolution algorithm written in Python
- Harmonic representations of the polarised beam response and sky to generate simulated CMB time-order data
- Arbitrarily shaped beams
- Ideal HWP modulation

UPGRADED *beamconv* VERSION (2021)

Duivenvoorden, Billi et al., MNRAS (2021)

In collaboration with A. Duivenvoorden, A. Adler, N. Dachlythra and Jón E. Guðmundsson we extended the capabilities of *beamconv* to include real HWP:

first time-domain simulations that include both HWP non-idealities and realistic full-sky beam convolution



We have been able to estimate the contamination of the BB power spectrum due to the interplay between dust modelling, beam and hwp non-idealities

DATA MODEL WITH BEAM CONVOLUTION AND HWP

WE MODEL THE TOD FOR A SINGLE DETECTOR OF A CMB POLARIMETER AS:

$$d_t = \int d\nu F(\nu) \int d\Omega(\hat{\mathbf{n}}) I_{\text{tot}}^{(t)}(\hat{\mathbf{n}}, \nu) + n_t$$

$$d_t = \underbrace{\left[S_{\text{instrument}} \right]}_{\text{Beam}} \left[M_{\text{rot},t} \right] \left[S_{\text{sky}} \right] \rightarrow \text{INNER PRODUCT OF INSTRUMENTAL STOKES VECTOR AND THE ROTATED sky STOKES PARAMETERS}$$

$$\left[S_{\text{beam}} \right] \left[M_{\text{HWP},t} \right]$$

FAR FIELD APPROXIMATION:

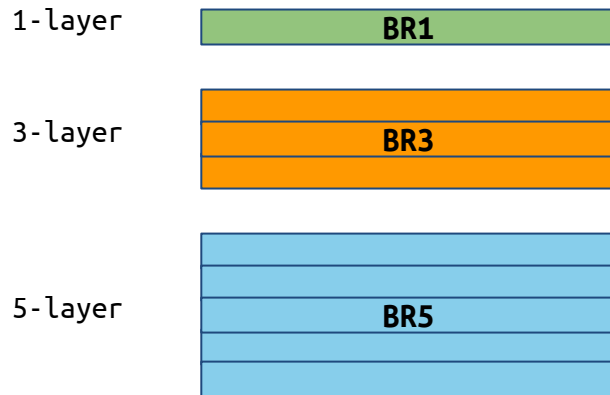
We factored the instrumental Stokes vector into a Stokes vector describing the beam response and a Mueller matrix describing the HWP. Ignores interaction between optics and HWP.

INSTRUMENT MODEL

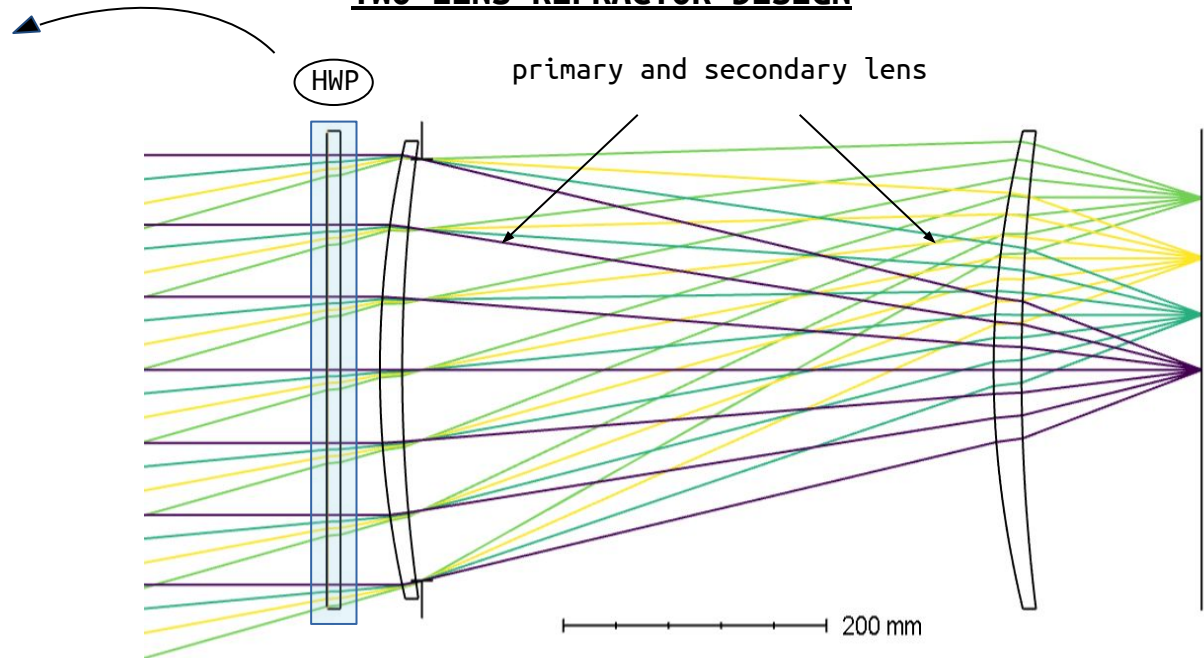
Time-domain simulation of a fiducial two-lens refractor telescope with an (achromatic) HWP

SKETCH OF TELESCOPE MODEL: TWO LENS REFRACTOR DESIGN

Different (achromatic) HWPs



The HWP is described the Mueller matrix.

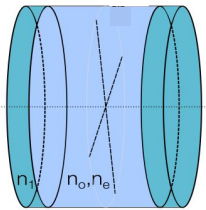


The telescope design defines the far-field beam response, expressed by the Stokes I, P, P*, V parameters

HWP MUELLER MATRIX

1-LAYER HWP CONFIGURATION

BIREFRINGENT PLATE



ANTI-REFLECTION COATING



1-layer HWP MUELLER MATRIX

$$\begin{pmatrix} T & \rho & 0 & 0 \\ \rho & T & 0 & 0 \\ 0 & 0 & c & -s \\ 0 & 0 & s & c \end{pmatrix}$$

IDEAL CASE: $T = -c = 1$; $\rho = s = 0$

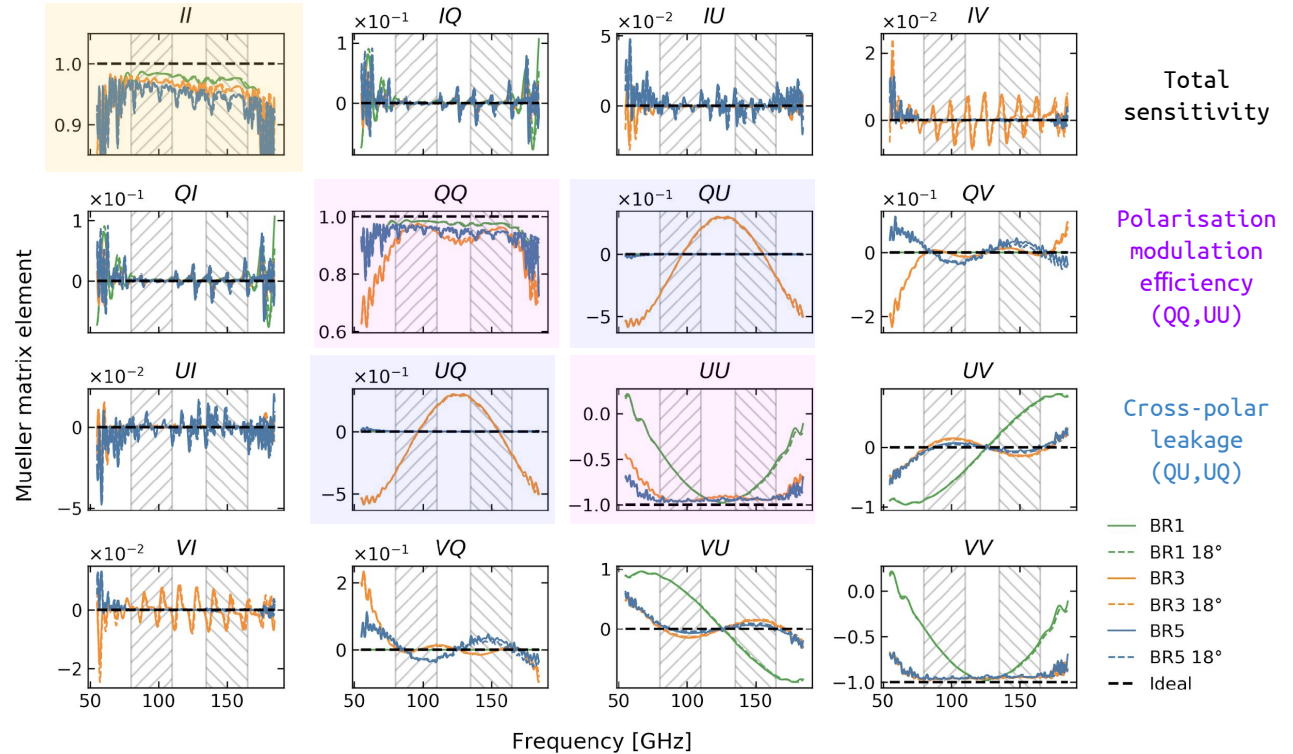
THREE HWP CONFIGURATIONS USED IN THE ANALYSIS:

BR1: ONE-LAYER HWP

BR3: THREE-LAYER AHWP

BR5: FIVE-LAYER AHWP

Achromatic HWP (AHWP)



Mueller matrices for arbitrary stacks calculated using T. Hileman's publicly available Code: <https://github.com/tomessingerhileman/birefringent-transfer-matrix>

FREQUENCY-INDEPENDENT DATA MODEL

WE CAN EXPRESS THE TOD MODEL IN THE HARMONIC DOMAIN AS:

$$d_t = \int d\nu F(\nu) \sum_{\ell, m, s} \left\{ b_{\ell s}^{\tilde{I}^{(0)}}(\nu, \alpha_t) a_{\ell m}^I(\nu) + b_{\ell s}^{\tilde{V}^{(0)}}(\nu, \alpha_t) a_{\ell m}^V(\nu) + \frac{1}{2} \left[-2b_{\ell s}^{\tilde{P}^{(0)}}(\nu, \alpha_t) a_{\ell m}^P(\nu) + 2b_{\ell s}^{\tilde{P}^{(0)}}(\nu, \alpha_t) a_{\ell m}^P(\nu) \right] \right\} \times \sqrt{\frac{4\pi}{2\ell+1}} e^{-is\psi_t} Y_{\ell m}(\theta_t, \phi_t) + n_t$$

HARMONIC MODES OF THE INSTRUMENT

$$b_{\ell s}^{\tilde{I}^{(0)}}(\nu, \alpha_t) = b_{\ell s}^{\tilde{I}_b}(\nu) C_{II}(\nu) + b_{\ell s}^{\tilde{V}_b}(\nu) C_{VI}(\nu) \\ + \underline{\text{Re}[b_{\ell s}^{\tilde{P}_b}(\nu) C_{P^*I}(\nu)] \cos(2\alpha_t) + \text{Im}[b_{\ell s}^{\tilde{P}_b}(\nu) C_{P^*I}(\nu)] \sin(2\alpha_t)}$$

→ Coupling to Stokes I of sky:
note the 2a terms

$$b_{\ell s}^{\tilde{V}^{(0)}}(\nu, \alpha_t) = b_{\ell s}^{\tilde{I}_b}(\nu) C_{IV}(\nu) + b_{\ell s}^{\tilde{V}_b}(\nu) C_{VV}(\nu) \\ + \underline{\text{Re}[b_{\ell s}^{\tilde{P}_b}(\nu) C_{P^*V}(\nu)] \cos(2\alpha_t) + \text{Im}[b_{\ell s}^{\tilde{P}_b}(\nu) C_{P^*V}(\nu)] \sin(2\alpha_t)}$$

→ Coupling to Stokes V of sky:
note the 2a terms

$$2b_{\ell s}^{\tilde{P}^{(0)}}(\nu, \alpha_t) = \underline{2b_{\ell s}^{\tilde{I}_b}(\nu) C_{IP}(\nu) e^{-2i\alpha_t} + 2b_{\ell s}^{\tilde{V}_b}(\nu) C_{VP}(\nu) e^{-2i\alpha_t}} \\ + \underline{2b_{\ell s}^{\tilde{P}^*_b}(\nu) C_{P^*P}(\nu) e^{-4i\alpha_t} + 2b_{\ell s}^{\tilde{P}_b}(\nu) C_{PP}(\nu)}$$

→ Coupling to Stokes Q/U of sky:
note the 2a and 0a terms

where:

$$b_{\ell s}^{(\tilde{I}/\tilde{P}/\tilde{P}^*/\tilde{V})_b} \quad \text{harmonic modes of the beam}$$

$$P = Q + iU \\ C = T M_{\text{HWP}} T^\dagger \longrightarrow T = \begin{pmatrix} 1 & 0 & 0 & 0 \\ 0 & \frac{1}{\sqrt{2}} & \frac{i}{\sqrt{2}} & 0 \\ 0 & \frac{1}{\sqrt{2}} & \frac{\sqrt{2}}{2} & 0 \\ 0 & 0 & 0 & 1 \end{pmatrix}$$

Note that ideal HWP

- Q, U modulated by $4\nu\alpha$ (HWP rot freq)
- I, V unmodulated

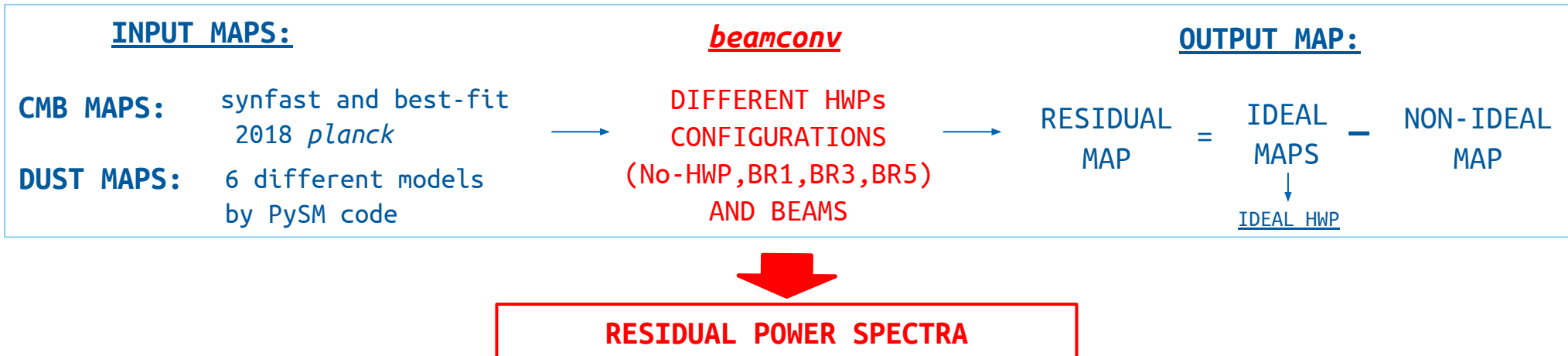
SIMULATIONS

TIME-DOMAIN SIMULATIONS OF A FIDUCIAL TWO-LENS REFRACTOR TELESCOPE WITH (ACHROMATIC) HWPS

SIMULATION SETUP:

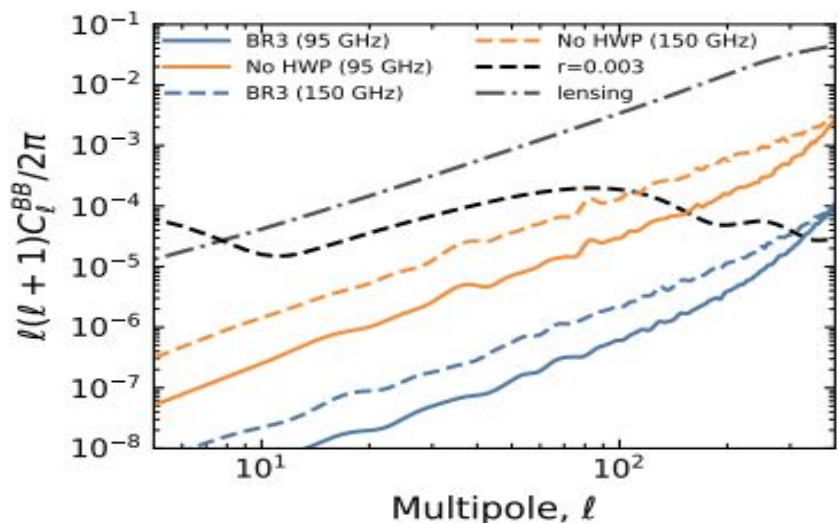
- 1-year satellite scanning with 50 dichroic detectors sensitive to two 30-GHz-wide frequency windows centred at 95 and 150 GHz;
- Detectors are distributed on a square grid of a focal plane fed by a 30-cm aperture telescope;
- In order to test frequency-dependent effects, we run simulations at seven sub-frequencies within a band (e.g. 80, 85, 90, 95, 100, 105, 110 GHz for the 95-GHz band)

PIPELINE

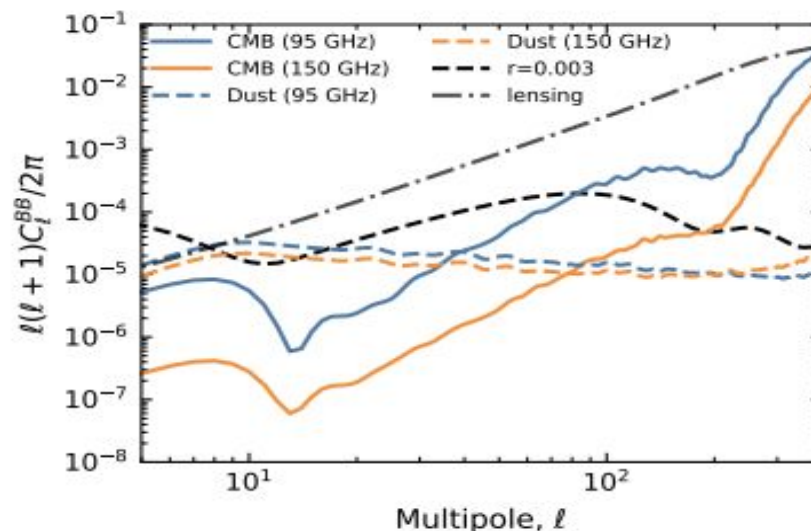


RESIDUAL POWER SPECTRA: GAUSSIAN BEAM

FOR THE 3-LAYER HWP, EACH SKY COMPONENT (CMB, DUST, ETC) NEEDS ITS OWN HWP ROTATION ANGLE CORRECTION:
BR3 EXHIBITS A ROTATION ANGLE OFFSET THAT VARIES ACROSS THE BAND AND DEPENDS ON THE SED OF THE SKY



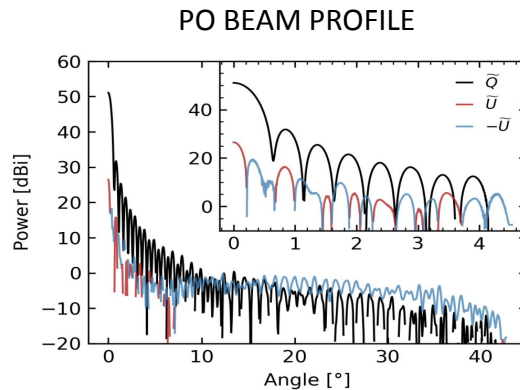
BR3 RESIDUAL B-MODE SPECTRA USING PHASE ANGLE FOR CMB WHEN OBSERVING CMB



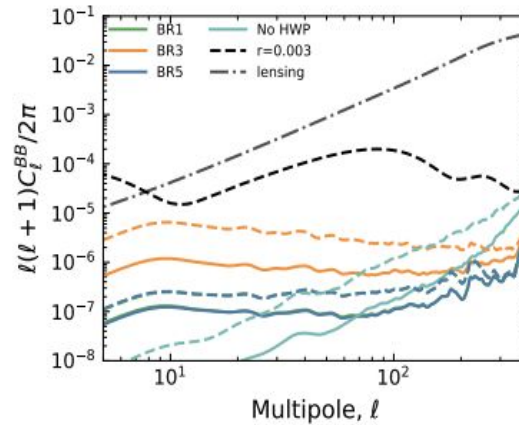
BR3 RESIDUAL B-MODE SPECTRA USING PHASE ANGLE FOR DUST/CMB WHEN OBSERVING CMB/DUST

RESIDUAL POWER SPECTRA: PHYSICAL OPTICS (PO) BEAM

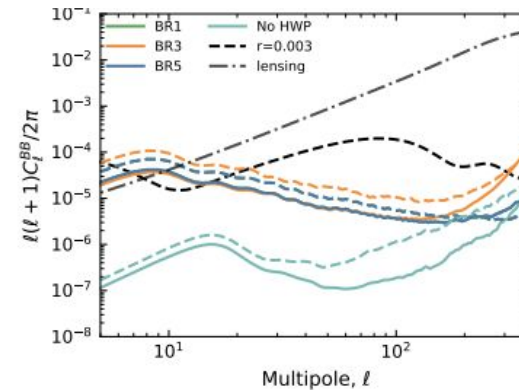
**HWP MODELS EXHIBIT RESIDUALS THAT MIGHT CONSTITUTE A SIGNIFICANT FRACTION OF THE SYSTEMATIC ERROR BUDGET:
BR3 RESIDUALS ARE COMPARABLE TO THE B-MODE AMPLITUDE ASSOCIATED WITH $r=0.003$**



Azimuthally averaged beam profiles for one of the 50 detectors used in this analysis.



RESIDUAL B-MODE POWER SPECTRA OF
DUST MODEL **d1** WITHOUT
FAR-SIDELOBES
(TRUNCATED AT 3°)



RESIDUAL B-MODE POWER SPECTRA OF
DUST MODEL **d1** WITH FAR-SIDELOBES
(TRUNCATED AT 30°)

SUMMARY

We formulated an extension of the publicly available code *beamconv* adding the capability of simulating systematics due to non-ideal HWPs. The generalised algorithm allows for generation of **simulated time-domain data that include spurious signal from non-ideal HWPs and physical optics polarised beams.**

We investigated three different HWP configurations, finding that depending on the complexity of Galactic foregrounds and the beam models, **certain HWP configurations significantly impact the B-mode reconstruction fidelity and could limit the capabilities of next-generation CMB experiments.** In particular we pointed out:

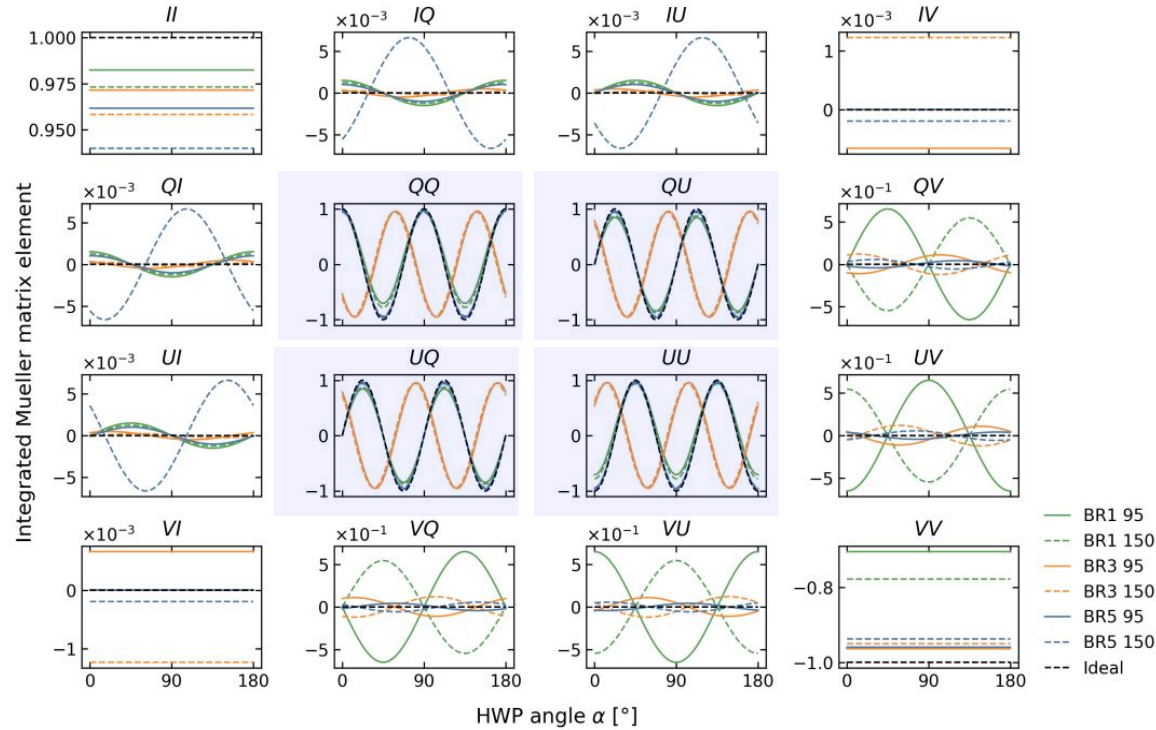
- the three-layer HWP that we studied comes with a significant frequency-dependent rotation angle offset, which, if not corrected for, acts as a polarisation angle offset that leaks E-mode to B-mode polarisation;
- there exist an interplay between the cross-polar component of the beam and certain HWP non-idealities. We found significant B-mode residual for all three HWP configurations when this interplay is not modelled correctly.

We can conclude that a thorough understanding of the instrumental beam will be necessary for current and future experiments attempting to model or correct for HWP non-idealities.

THANK YOU FOR YOUR ATTENTION!

EXTRA SLIDES

Determining the AHPW induced rotation offset



MM elements for the three HWP configurations integrated over the frequency bands: 95 GHz (solid lines) and 150 GHz (dashed lines) as a function of the HWP rotation angle. The dashed black lines represent the behaviour of the ideal HWP. It can be seen that the BR3 configuration (orange lines) is out of phase with the other HWP configurations.

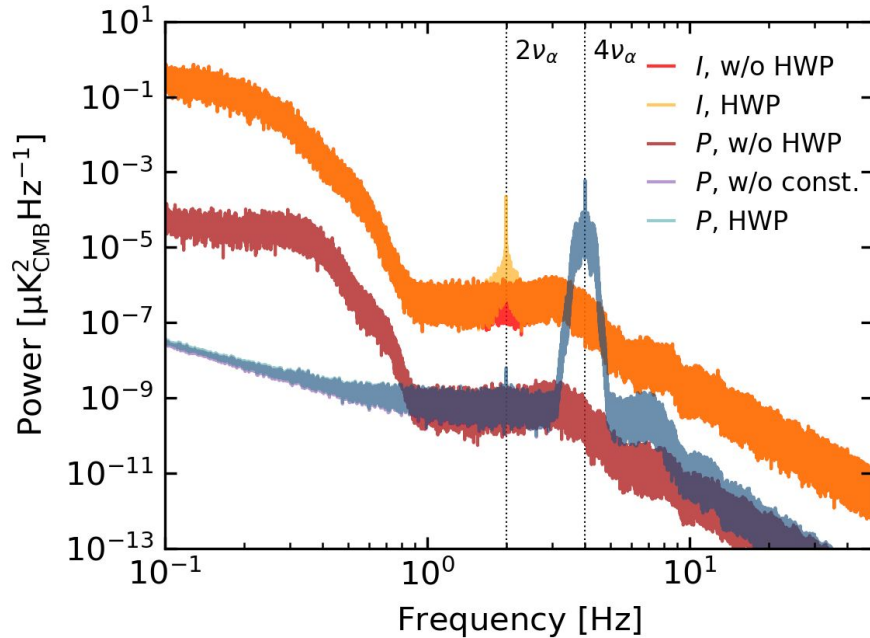
We can determine an optimal rotation angle offset for a specific sky component as the HWP rotation angle that minimizes the difference between the QQ , QU , UQ , UU submatrices of the Mueller matrices of the HWP and the ideal HWP.

$$R(\alpha) = \sum_{i,j \in \{Q,U\}} \left[\sum_{k=1}^{n_\nu} w(\nu_k) M_{\text{HWP},ij}(\nu_k) - D_{ij}(\alpha) \right]^2$$

↓

weights applied to model the SED

Power spectral densities



An ideal HWP modulation will only modulate the Q and U sky signal, which it will do at a modulation frequency $4\nu_\alpha$.

Non-ideal HWP introduces:

- a $2\nu_\alpha$ modulation of the I sky
- a $2\nu_\alpha$ modulation of the V sky
- a $2\nu_\alpha$ modulation of the Q and U sky and
- a constant $0\nu_\alpha$ modulation of the Q and U sky

Power spectral densities (PSDs) corresponding to a typical two-hour segment of noiseless TOD for a single detector. The curves labelled I (P) correspond to scans over an I-only ((Q, U)-only) simulated CMB sky. The curves labelled HWP include HWP modulation using the three-layer BR3 HWP configuration spinning at a frequency of 1 Hz. The curve labelled P, w/o const. (Overlapping with P, HWP but slightly different below ~ 2 Hz) incorporates the same HWP modulation, but does not include the HWP systematic that is constant with HWP angle α . The curves labelled w/o HWP do not include HWP modulation.